Surface Texture

J.F. Song and T.V. Vorburger, National Institute of Standards and Technology

TRIBOLOGISTS are concerned with what happens when two solid surfaces slide over each other, under either dry or lubricated conditions. They often measure and compare the surface texture and roughness parameters before and after the wear process, and at intermediate stages as well. Understanding the relationship between wear properties and surface texture can lead to the specification of optimized surface textures and manufacturing processes for various surface function needs.

The term "surface texture" refers to the fine irregularities (peaks and valleys) produced on a surface by the forming process. By convention, the texture comprises two components: roughness and waviness. Roughness consists of the finer irregularities characteristic of the process itself, such as the grit spacing of a grinding wheel or the feed of a single-point tool. Waviness consists of the more widely spaced irregularities that are often produced by vibration in the machining process. Usually, however, the terms "surface texture" and "roughness" are used interchangeably, because roughness is specified and measured much more often than waviness. The surface topography includes these surface texture components as well as any other irregularities, such as error of form.

There are two types of profiling techniques for surface texture, depending on whether the height measurements are made simply along a line (profile methods) or over an area (raster area methods). Both types of techniques develop quantitative knowledge of the surface peaks and valleys by point-by-point measurement with a high-resolution probe. Surface profiles are generally measured across the surface lay, the direction of uniaxial machining marks caused by most surface forming processes. The profile may be produced by a contacting stylus that traverses the surface, by a noncontacting probe, or by optical interferometric fringes. The stylus method has been widely used (Ref 1-10) by engineers, opticists, and tribologists. Therefore, the stylus technique will be discussed in some detail in this article as an important example of surface profiling. Other techniques are discussed elsewhere (Ref 11, 12).

Surface Statistics

In general, surface textures are highly complex, because many surface finishing processes, such as polishing, grinding, and shot blasting, are statistical by nature. To characterize such surfaces, two types of statistical descriptors are used: parameters, such as root mean square (rms) roughness, which attempt to quantify some aspect of the surface statistics with a single number, and statistical functions, such as the power spectral density, which by their nature yield an array of information about the surface.

Surface Parameters

There are a great variety of surface parameters, many of which have been developed to characterize the function of engineering surfaces for particular applications. In fact, about 50 to 100 parameters have been defined for industrial use, and many of these appear in national standards as well. Nevertheless, surface parameters can generally be classified as height parameters, wavelength parameters, shape parameters, and combinations of these, known as hybrid parameters.

Height Parameters. The most common statistical descriptors of surface height are the roughness average, R_a, and the rms roughness (also called R_q). These are closely related and are given by the following formulas, shown in integral and digitized form:

$$R_a = \frac{1}{L}\int_0^L |y(x)|\,dx = \frac{1}{N}\sum_{i=1}^{N} |y_i| \qquad \text{(Eq 1)}$$

$$R_q = \left[\frac{1}{L}\int_0^L y^2(x)\,dx\right]^{1/2} = \left[\frac{1}{N}\sum_{i=1}^{N} y_i^2\right]^{1/2} \qquad \text{(Eq 2)}$$

where $y(x)$ is the surface profile, sampled by the set of N points y_i over the length, L, as shown in Fig 1. The parameters R_a and R_q are useful estimators of the average heights and depths of surface profiles. The rms roughness is commonly specified for the surfaces of optical components. In general, the lower the rms roughness of an optical component, the less stray scattered light and thus the higher the quality of the component. Roughness average is used in the automotive and other metalworking industries to specify the surface finish of many types of components, ranging from cylinder bores to brake drums (Ref 13). In addition to these two averaging height parameters, an assortment of other height parameters have been defined for various applications, including several for characterizing peak-to-valley height (Ref 4, 14).

Wavelength parameters are used to characterize the spacings of the peaks and valleys of the surface. The spacings or wavelengths are often characteristic of the process that formed the surface, such as the shot size used for abrasive blasting, the grit size of a grinding wheel, or the feed of a tool. A typical wavelength parameter, recognized as standard by the International Organization for Standardization (ISO), is the mean peak spacing S_m (Ref 14), defined for a surface profile as the average spacing between two successive negative crossings of the mean line (see Fig 2).

Shape Parameters. The periodic profiles in Fig 3 all have the same R_a and wavelength, but have different shapes and thus may perform differently in different applications. In particular, the profile in Fig 3(b) represents a good load-bearing surface, and the profile in Fig 3(a) represents a poor one. Because of its facets, the profile in Fig 3(c) is best used as a diffraction grating, whereas one of the other surfaces may be most suitable for lubricated sliding. Shape parameters help to quantify the differences between these surfaces. The most important parameter, the skewness, is a measure of the symmetry of the profile about the mean line. It is defined as:

$$R_{sk} = \frac{1}{NR_q^3}\sum_{i=1}^{N} y_i^3 \qquad \text{(Eq 3)}$$

According to this definition, the skewness of the profile in Fig 3(a) is positive, whereas its oppo-

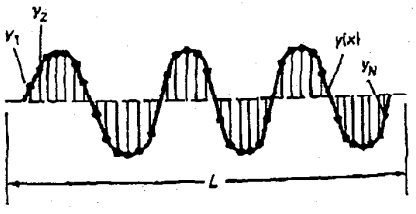

• R_a = Average absolute deviation of profile $y(x)$ from the mean line = total shaded area/L

Fig 1 Idealized stylus profile showing the mean line; the evaluation length, L; the digitized points, y_i; and a definition of the parameter R_a

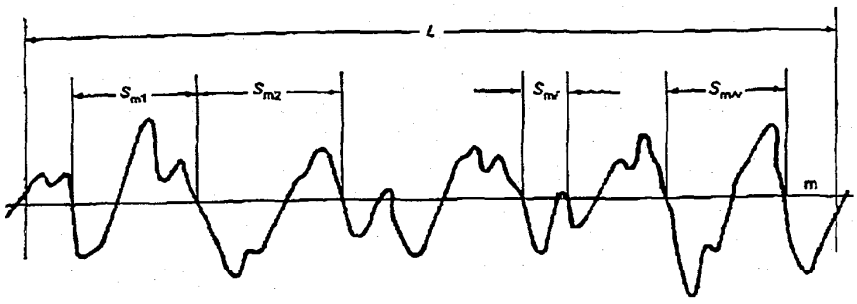

$$S_m = \frac{1}{n}\sum_{i=1}^{n} S_{mi}$$

Fig 2 Surface profile showing the ISO definition for the peak spacing parameter, S_m

site number (Fig 3b) has negative skewness. The other two profiles (Fig 3c and d) are symmetrical and have zero skewness.

Hybrid Parameters. Slope and curvature are two examples of quantities that combine the concepts of height deviation and lateral displacement and are thus termed hybrid parameters. They may be defined analytically or digitally in several ways. Hybrid parameters have been used in a number of areas of tribology, such as theories describing elastic contact (Ref 15) and thermal contact conductance (Ref 16).

Statistical Functions

More complete statistical descriptions of the properties of surface profiles can be obtained from statistical functions, such as those used in random process theory and time series analysis (Ref 17-19). Four important statistical functions are the amplitude density function or height distribution, the bearing area curve, the power spectral density, and the autocorrelation function. The definitions and applications of these functions are described in several sources (Ref 2, 6, 7, 17-23). The power spectral density and the autocorrelation function will be discussed in detail here.

The power spectral density (PSD) decomposes the surface profile into its spatial Fourier component wavelengths. It is given analytically by:

$$\mathrm{PSD}(F) = \lim_{L\to\infty}\left(\frac{1}{L}\right)\left|\int_0^L y(x)\cdot e^{-2i\pi Fx}dx\right|^2 \qquad \text{(Eq 4)}$$

and is estimated in digitized form by:

$$\mathrm{PSD}(F) = \mathrm{PSD}(k) = \frac{1}{N\Delta}\left|\sum_{j=1}^{N} y(j)\cdot e^{-2i\pi kj/N}\right|^2 \qquad \text{(Eq 5)}$$

In Eq 4 and 5, Δ is the lateral point spacing (sampling interval) of the digitized data points, the total length of the profile, L, is equal to $N\Delta$, and the set of spatial frequencies, F, in the digitized PSD is given by k/L, where k is an integer that ranges from 1 to $N/2$. Calculation of the digital Fourier transform in Eq 5 can be greatly speeded by using fast Fourier transform (FFT) algorithms (Ref 24, 25).

Figure 4 illustrates the sensitivity of the PSD to the different characteristics of surfaces produced by different processes. Figure 4(a) shows the PSD plotted for a highly sinusoidal surface, a prototype of those available from the National Institute of Standards and Technology (NIST) as standard reference materials (Ref 26, 27). The Fourier amplitude at the fundamental frequency of 0.01 μm^{-1} (wavelength = 100 μm, or 10^6 Å) is the dominant feature in the curve, but imperfections in the sinusoidal nature of the surface are also evident from the presence of higher harmonics in the spectrum. By contrast, Fig 4(b) shows a more random surface produced by the grinding process and its PSD (Fig 4c) that has a fairly decaying, albeit somewhat randomized, distribution, with little evidence of periodic components.

Autocovariance and Autocorrelation. The complementary function to the power spectral density is its Fourier transform, the autocovariance function, $C(\tau)$:

$$C(\tau) = \int_{-\infty}^{\infty} [\mathrm{PSD}(F)]e^{2i\pi F\tau}\,dF \qquad \text{(Eq 6)}$$

Alternatively, the autocovariance function can be calculated directly from the profile itself. That formula is given by an overlap integral of shifted and unshifted profiles:

$$C(\tau) = \frac{1}{L}\int_0^L [y(x)][y(x+\tau)]dx \qquad \text{(Eq 7)}$$

where the quantities L and $y(x)$ have been defined previously.

The value of the autocovariance function at zero shift ($\tau = 0$) is by definition equal to the mean square roughness, R_q^2, of the profile, provided an appropriate mean line has been subtracted from the profile to calculate $y(x)$. When the autocovariance function is normalized by dividing by the zero shift value, the result is known as the autocorrelation function (ACF), $c(\tau)$:

$$c(\tau) = \frac{C(\tau)}{R_q^2} = \frac{\int_0^L [y(x)][y(x+\tau)]dx}{\int_0^L [y^2(x)]dx} \qquad \text{(Eq 8)}$$

If the fact that the overlap between the shifted and unshifted profiles decreases as the shift distance increases for a finite length profile is taken into account and the digital formulation is simultaneously used, the ACF can be estimated by:

$$c(\tau) = \left(\frac{1}{N-j}\right)\left(\frac{\sum_{i=1}^{N-j}[y(i)][y(i+j)]}{\sum_{i=1}^{N} y^2(i)}\right) \qquad \text{(Eq 9)}$$

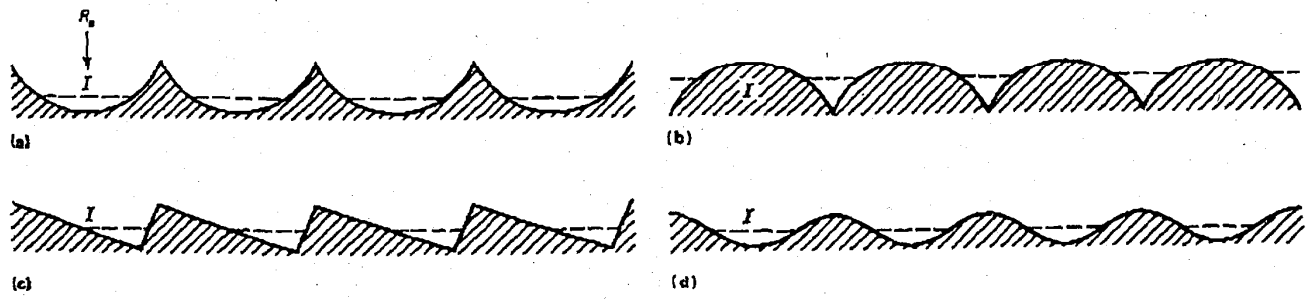

Fig 3 Profiles for four different surfaces with the same roughness average, R_a, and wavelength but varying skewness, R_{sk}. (a) $R_{sk} > 0$. (b) $R_{sk} < 0$. (c) $R_{sk} = 0$. (d) $R_{sk} = 0$. The dotted line shows the position of the mean value.

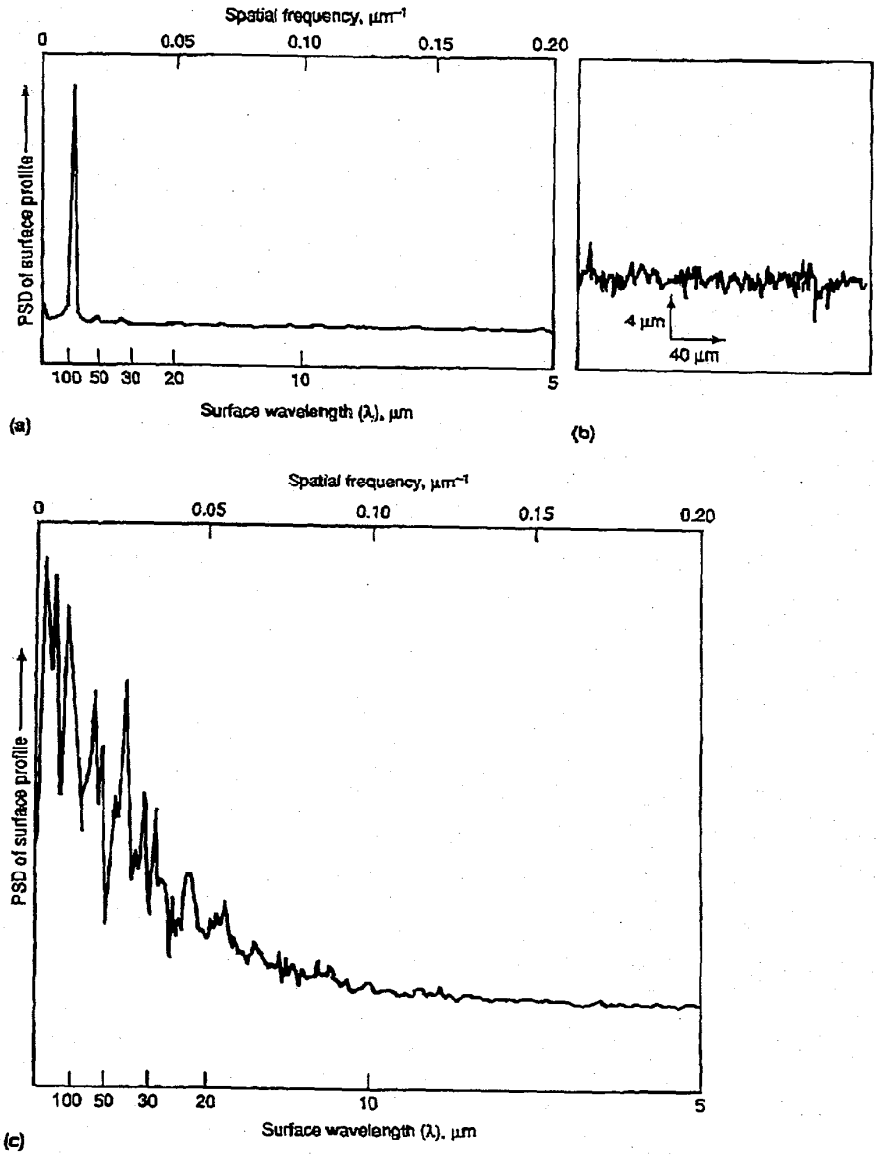

Fig 4 Power spectral density functions for profiles of two roughness specimens. (a) Sinusoidal roughness specimen machined by diamond turning with R_a of 3 μm (120 μin.) and spatial wavelength of 100 μm (10^6 Å). (b) Roughness profile of a commercially ground surface whose PSD is shown in (c). (c) Commercially available specimen of a ground surface with R_a of 0.6 μm (24 μin.). Both power spectra are calculated for profiles having trace lengths of 3.0 mm (0.15 in.). The ordinate values are equal to the square root of the power spectral density values and are plotted in arbitrary units.

The autocovariance and autocorrelation functions are useful for visualizing the relative degrees of periodicity and randomness in surface profiles. For example, Fig 5 shows ACFs for germanium and silicon surfaces calculated from surface profiles measured by a stylus instrument (Ref 28). Both surfaces were machined by diamond turning under similar conditions, but the periodicity imposed by the feed of the tool was much stronger on the silicon surface and thus its ACF is highly periodic. Because of its more random surface topography, the germanium surface exhibits a strongly decaying ACF, with only a small amount of periodicity shown as a barely visible oscillation.

Therefore, as measures of the lateral structure of surfaces, the PSD and the ACF seem to be useful in different ways. The PSD is useful for studying the strengths of various periodic components in the surface profile and for comparing these with the strength of the broad spectrum of random components. The ACF is useful for observing directly the lateral extent of the random structures on the surface by studying the decay in the function near zero shift.

Other Descriptors

As stated previously, scores of parameters and functions have been developed to quantify stylus profiles of surfaces, many of these for applications in tribology and engineering. The choice of roughness parameters and/or statistical functions to characterize the surface function adequately is critical for each application. An example from the automotive industry will be discussed here.

Finishing of engine cylinder bores by the plateau honing process (Ref 29) may result in an optimal cylinder bore surface texture. This surface has a negative skewness, R_{sk}, which results in good performance for running-in, long-term running, and lubrication of the cylinder bores. In such situations, the traditional roughness parameter, R_a, does not adequately estimate the performance of cylinder bore surfaces. The deep valleys, which can be used as oil reservoirs during engine operation, are better quantified by combining R_a with R_{sk}. Indeed, other parameters, such as the R_k family (Ref 30), have also been developed as functional descriptors of these types of surfaces.

Therefore, it may be possible to optimize the functional performance of engineering surfaces by combining the specification of surface texture parameters, material, and manufacturing process with the development of quality control procedures. This combination has been called "surface texture design" (Ref 31).

It is likely that in surface science, too, other topographic parameters can be developed that correlate well with performance. For example, Blakely and Somorjai (Ref 32) and others correlated the ability of a surface to foster certain surface chemical reactions with the presence of lattice steps on the surface. These ideas could be quantified in terms of a step density parameter that might be defined as the fraction of surface atoms that are adjacent to lattice steps.

Experimental Issues for Stylus Instruments

The height resolution and range of stylus instruments depend largely on two factors: the transducer and the mechanical noise and straightness of the traverse mechanism. In many research instruments, the transducer is a linear variable differential transformer (LVDT) (Ref 3) that, together with demodulation and amplification circuitry (Ref 33), produces an output directly proportional to surface height. Another type of transducer based on optical interferometry also produces a signal directly proportional to height (Ref 34). Inductive and piezoelectric transducers that are sensitive to the vertical motion of the stylus (that is, the time derivatives of the stylus tip height rather than the height itself) are also available (Ref 33, 35). These types are generally more economical than LVDTs and are

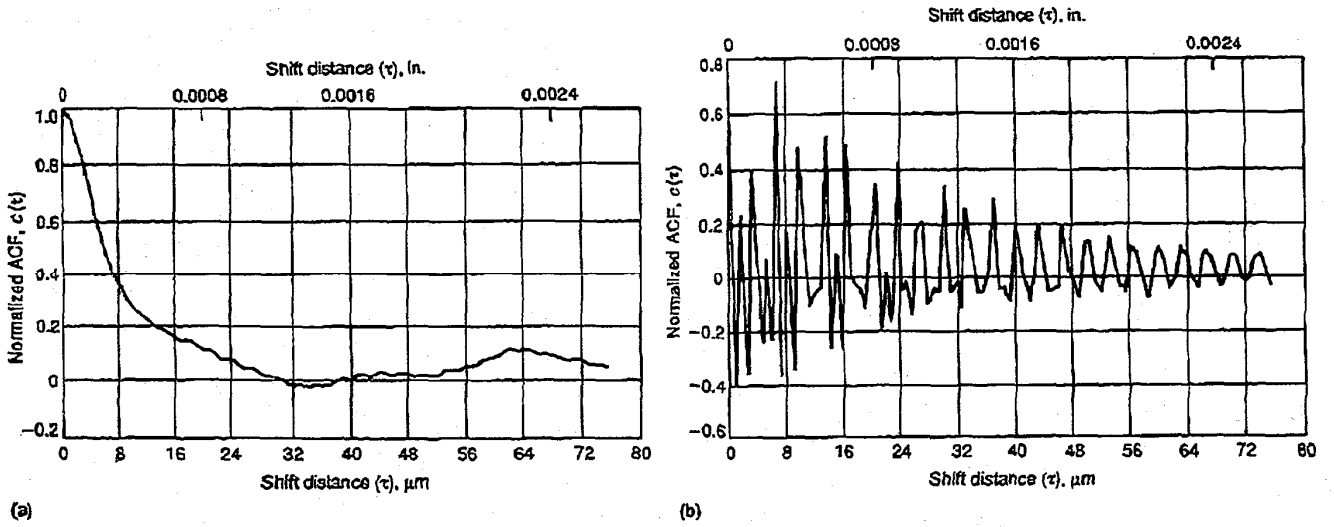

Fig 5 Autocorrelation functions for single-crystal surfaces machined by diamond turning. (a) Germanium. (b) Silicon. The curve for germanium is an average of three ACFs measured at different positions on the surface. For silicon, the curve is an average of four ACFs.

more generally used in industrial shops than in research or metrology laboratories.

An example of an LVDT is shown schematically in Fig 6. As the stylus moves vertically, the ferrite core is displaced from the balance position of an alternating current (ac) bridge, to which the coils are connected, and which is driven at a high carrier frequency. The out-of-balance voltage signal that is demodulated and amplified is proportional to the vertical displacement of the stylus. Some transducers are so sensitive as to have rms noise levels of about 0.1 nm (Ref 7), which means that surface structures approximately one atom high can be detected. Other LVDT transducers have vertical range as large as several hundred micrometers or more, and, in general, the ratio of range to resolution is on the order of 10^5. One version of the optical transducer (Ref 34) mentioned above has an even wider range (~4 mm, or 0.16 in.) and a resolution of approximately 0.01 μm.

Three types of designs for achieving low scanning noise and good straightness of travel are shown in Fig 7. The least expensive method involves the use of a skid (Fig 7a), which traces a reference line on the surface very near to the LVDT. The vertical position of the stylus is measured with respect to the path of the skid. The skid also serves as a high-pass mechanical filter because it averages over a fairly wide swath of surface peaks. Mechanical noise in the drive mechanism can be significantly reduced by this approach, because such noise does not couple well into relative motion between the stylus and the skid to which it is referenced.

Figure 7(b) schematically shows an external reference datum surface that guides the motion of the tracer. Well-engineered tracing systems may minimize the Abbé offset (Ref 36) between the reference surface and the measured surface by placing the stylus contact and the set of reference contacts as close to the same vertical line as possible. Alternatively, such systems may minimize the amount of angular motion and vibration in the carriage.

The design shown in Fig 7(c) involves no sliding components at all. Rather, a flexure pivot or a set of pivots constrains the motion to a plane that is perpendicular to the axis of the pivot. The solid construction provides highly noise-free motion. One commercial design has been shown to provide approximately 0.1 nm rms noise (Ref 7) over a trace length of 1 mm (0.04 in.). Another variation of the flexure approach (Ref 37) involves multiple sets of flexures to allow for motion in two directions.

For measurements of smooth surfaces that require high vertical magnification, the straightness error of the traverse mechanism can seriously distort the measured profile. Figure 8(a) shows a distorted profile of a 91 nm (3.6 μin.) step-height specimen (Ref 31). The use of the skid can substantially eliminate this error (see Fig 8b), because the reference datum is a portion of the surface located very close to the stylus. This consideration is closely related to the Abbé principle in dimensional measurement (Ref 36). The skid approach works well as long as the skid is traversing on a smooth reference surface. However, use of the skid can lead to unwanted distortions in the profile, particularly in cases

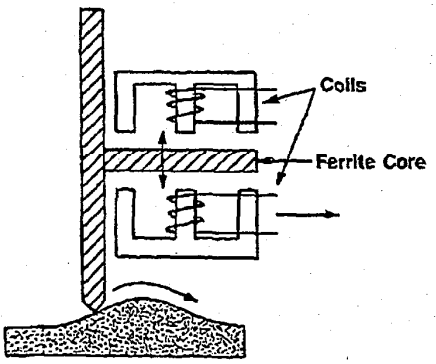

Fig 6 Schematic showing key components of a high-sensitivity LVDT. As the stylus traverses the peaks and valleys of the surface, the ferrite core moves vertically with respect to the coils.

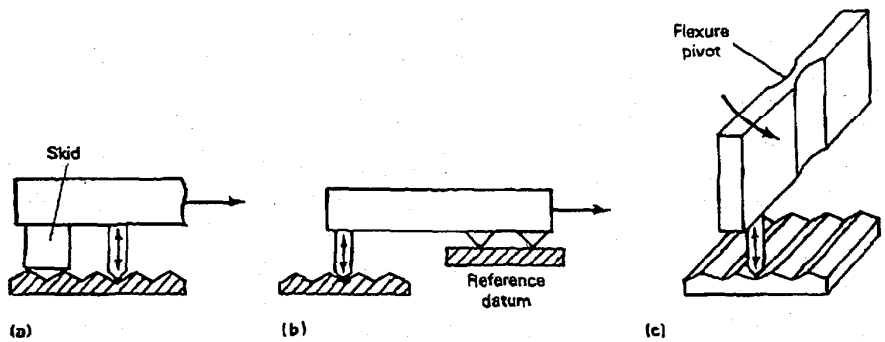

Fig 7 Schematic showing three types of configurations used to constrain unwanted motion of the stylus. (a) High-pass mechanical filter skid. (b) External reference datum to guide tracer motion. (c) Flexure pivot setup

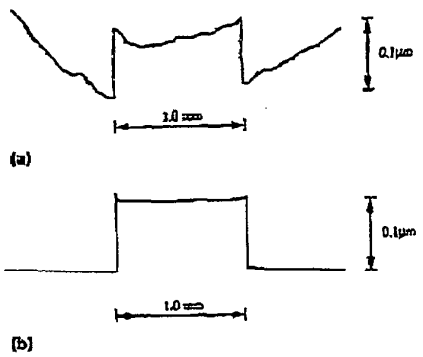

Fig 8 Profile of a 91 nm (3.6 μin.) step-height specimen distorted by the straightness error of the traverse mechanism of the stylus instrument. (a) Stylus without skid. (b) Stylus with skid

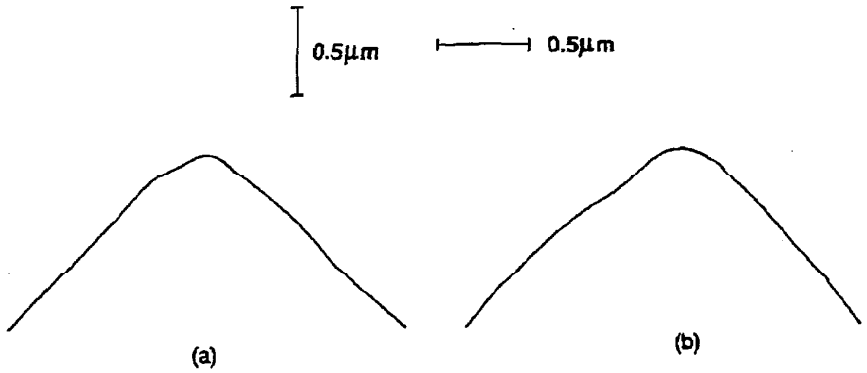

Fig 10 Profile graph of low-usage stylus related to profile graph of identical stylus after 15 months of service (a) Measured in March 1988 with a tip width of approximately 0.05 μm (2 μin.). (b) Measured in June 1989; width is approximately 0.15 μm (6 μin.) after dozens of traces.

where the surface contains isolated peaks (Fig 9). Another problem with skids is the potential for surface damage, because the skid loading on the surface may be hundreds of times larger than the stylus force.

Lateral Resolution and Range. The drawback of flexure designs is that the trace length is limited by the degree to which the flexure may be bent before the elastic bending forces become too large. In the two designs discussed above, that trace length limit is about 2 to 3 mm (0.08 to 0.12 in.). However, as a rule, lateral range is not a problem for stylus instruments. The lead-screw drive mechanisms of many instruments permit trace lengths on the order of 100 mm (4 in.) or more.

Because a stylus profile represents the convolution of the surface structure with the end form of the stylus, the lateral resolution depends critically on the size of the stylus tip and to a lesser degree on the flank angle. Styli are often flattened at the end, the width across the flat essentially determining the lateral resolution. A commonly available width is 2 μm (80 μin.), but pyramidal styli with tips as small as a nominal 0.1 × 0.1 μm (4 × 4 μin.) are also used. In some instances, highly spherical styli are also produced. Bennett and Dancy (Ref 7) and Vorburger *et al.* (Ref 38) show micrographs for these. Figure 10(a) shows a stylus with a tip width of ~0.05 μm as measured by the razor blade tracing technique (Ref 38, 39). One year later, after dozens of traces, the profile graph of the same stylus (Fig 10b) shows a certain amount of wear, because the width has increased to approximately 0.15 μm (6 μin.).

If the stylus tip is spherical, the lateral resolution can be smaller than the tip radius, r. Figure 11 shows the geometrical construction when a spherical stylus first contacts a step, which is assumed to be infinitely sharp. If $h \ll r$, the point of initial contact occurs at a position $\sqrt{2hr}$ to the left of the step edge; thus, $\sqrt{2hr}$ represents the width of the transition and the effective resolution of the stylus. The calculation assumes that no deformation occurs at the single point of contact. In the case of a 1 μm (39 μin.) radius stylus and a step of height 10 nm, the calculated transition width is 0.14 μm (5.5 μin.).

The flank angle of the stylus (Fig 11) also affects its resolution. The stylus cannot accurately profile over slopes greater than the flank angle (usually ±45°). This is not a problem for most types of smooth surfaces where the average surface slopes are only a few degrees, but it does complicate measurements of surfaces with steep cracks or holes, such as those on ceramics or cast materials.

An example of the lateral resolution capability of a stylus instrument is illustrated in Fig 12(a) (Ref 39), which shows a profile of a 6000 lines/mm grating measured using a flexure-pivot-type stylus instrument with a 0.05 μm (2 μin.) tip width (Fig 10a) and 0.6 μN stylus loading. A piezoelectric stage was used to drive the surface under the stylus to obtain the high lateral magnification. By contrast, Fig 12(b) shows a profile of the same surface with a much wider (0.5 μm, or 20 μin.) stylus tip.

To summarize, the convolution of the stylus with the surface reduces the widths of valleys and increases the widths of peaks in the output profile. The minimum detectable valley width is roughly equal to the stylus tip width itself, but may be smaller for spherical styli tracing over very shallow valleys. From geometrical arguments, the minimum detectable peak width can be quite small in principle, but if it becomes considerably smaller than the stylus tip width, the area of contact would be decreased, the stylus pressure would increase, and the stylus might tend to deform such an asperity. However, peak spacings of 0.05 μm (2 μin.) have been detected (Ref 39) on the surfaces of random-profile precision roughness specimens (Ref 40) using commercially available stylus tips.

Bandwidth Limits for Surface Metrology. The foregoing discussion leads to the important concept of bandwidth limits (Ref 28) for surface metrology. Stylus instruments are sensitive to a certain bandwidth of surface spatial frequencies, limited at the high-frequency end by the stylus width and the sampling interval and at the low-frequency end by the traverse length or by high-pass electrical filtering. One of the most important considerations in stylus profiling is whether or not the wavelength domain of interest on the measured surface falls in the flat portion of the transmission function of the instrument. For example, at position X in Fig 13 (Ref 41), there is essentially no attenuation caused by the factors that limit either range or resolution. One type of instrument has a traverse of 2.5 mm (0.1 in.) and can employ stylus tips having widths as small as 0.1 μm (4 μin.). Therefore, the effective bandwidth of spatial wavelengths sensed by this instrument extends over the range of approximately 0.1 to 2500 μm (4 to 10^5 μin.) for its unfiltered operation. For many industrial appli-

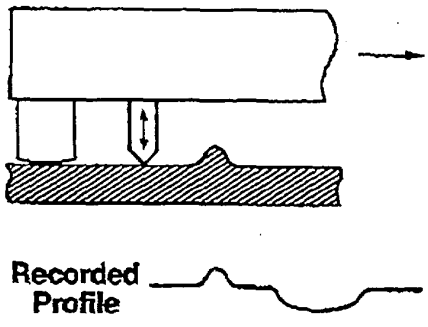

Fig 9 Schematic showing an isolated peak on the specimen surface generating a false valley in the profile that was measured by a stylus instrument incorporating a skid

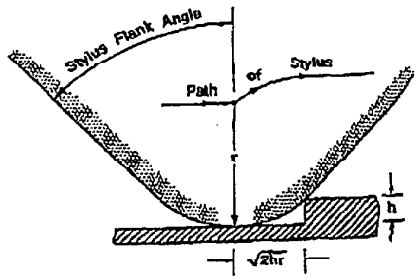

Fig 11 Schematic showing the path traced by spherical stylus tip traversing over a small sharp step

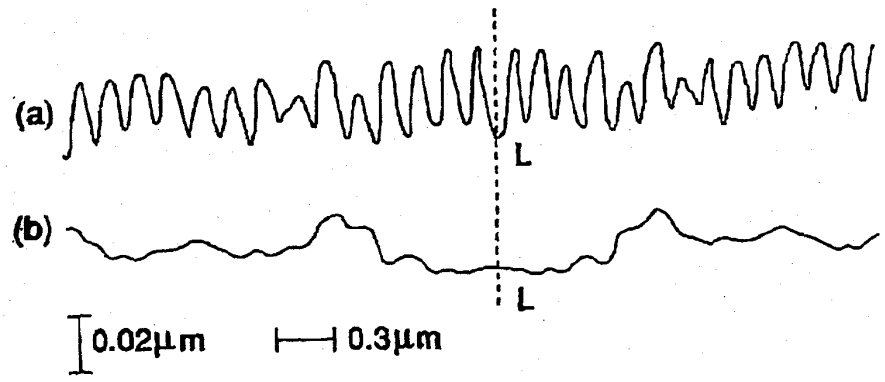

Fig 12 Surface structure of the 6000 lines/mm grating recorded by a flexure-pivot-type stylus under a 0.6 μN load. (a) Measured by a 0.05 μm (2 μin.) width stylus. (b) Measured by a 0.5 μm (20 μin.) width stylus

cations, the standard stylus has a radius of 10 μm (400 μin.) and the long-wavelength cutoff (λ_c) is determined by a standard high-pass electrical filter that is often set to 800 μm (3×10^4 μin.). The spatial wavelength bandwidth of these instruments extends approximately over 10 to 800 μm (400 to 3×10^4 μin.). Spatial wavelengths larger or smaller than this range are detected with reduced or nil sensitivity.

It is important for the operator to use a bandwidth that encompasses the spacing of the surface roughness structures to be evaluated. This means that, on the one hand, the finest surface features to be assessed must be more widely spaced than the stylus tip width or radius and, on the other hand, that the nominal instrument cutoff must be several times longer than the most widely spaced features to be assessed.

However, the bandwidth also affects the rms noise of the measurement. The wider the bandwidth, the more noise enters into the output profile. The noise contribution to a roughness measurement can be checked for most stylus instruments by measuring an optical flat, because such a specimen ordinarily has a roughness that is smaller than the noise resolution of the instrument. The resulting value of measured R_a or R_q represents the noise resolution of the instrument, including both the mechanical noise of traversing and the electrical noise over the finite spatial bandwidth as discussed above.

Stylus Load and Surface Deformation. The logical parameters that determine whether surface damage will be caused by stylus load are the surface hardness, the stylus force, the stylus tip width, and, to a lesser extent, the stylus speed. A stylus tip width of 1 μm (40 μin.) should not produce detectable damage on metal surfaces as soft as gold as long as the stylus force is smaller than about 0.03 mN.

Many types of stylus instruments use stylus forces of 0.5 mN and higher, but these are normally used with stylus tip sizes on the order of 10 μm (400 μin.). Because the pressure is inversely proportional to the area of contact, the pressure on the surface caused by stylus loading is smaller for a 10 μm (400 μin.) stylus with a 0.5 mN force than it is for a 1 μm (40 μin.) stylus with a 0.03 mN force. Even if the stylus leaves a visible track, the resulting profile is likely to be accurate, because the variation in the depth of the track over the surface should be significantly smaller than the depth itself. However, if a skid is used for stylus profiling, the measured surface can be seriously damaged by the skid, whose loading is hundreds of times larger than the stylus loading.

The above discussion pertains only to plastic or irreversible deformation of the surface by stylus loading. Characterizing the elastic or reversible deformation (Ref 6) is much more difficult, but the elastic deformation is expected to be very small (Ref 42).

In a study of plastic damage, Song and Vorburger (Ref 39) measured a 2160 lines/mm gold grating with a 0.5 μm (20 μin.) stylus tip width. When the stylus loading increased from 0.6 to 100 μN, the grating profile in the same position was attenuated (Fig 14a-d). When the stylus loading was reduced again to 0.6 μN (Fig 14e), most of the periodic structure of the profile in Fig 14(a) had been plastically eliminated by the previous loading conditions and did not reappear. However, a few of the fine peaks did reappear, and the difference between the profiles in Fig 14(d) and (e) suggests that some features were only elastically deformed by the increased stylus loading.

Other Distortions. Stylus flight (Ref 43-45) and profile digitization are two other sources of profile distortion. Stylus flight can occur when the stylus encounters a sharp change in the surface topography, such as a steeply rising surface step. The logical parameters that affect this phenomenon are the stylus speed, the stylus force on the surface, the stylus tip size, the damping constant in the vertical direction, and the rate of change of the surface slope. A key tradeoff occurs between stylus force and speed. A magnetic phonograph cartridge with a force of 20 mN can have a record disk traverse beneath it at a tangential speed of 500 mm/s (20 in./s) without losing contact, but a stylus with a force of 0.1 mN must travel much more slowly, about 1 mm/s (0.04 in./s), to maintain contact. The usual symptom of stylus flight is a peak in the measured profile with a sharp rise and slower fall occurring after the stylus encounters a sharp peak on the surface. The accuracy of such features can be verified by remeasuring the same profile at a slower speed.

Stylus profiles are routinely digitized for the purposes of computer processing and mass storage. In order to obtain an accurate digital representation of the profile, the peak-to-valley height of the profile should consist of many vertical quantization levels, and the widths of the surface features to be studied should consist of many lateral sampling intervals. In addition, if the distribution of surface peaks and valleys is being characterized, there should be enough points in the profile to give an adequate statistical sampling of the variability of these structures. The system at NIST used 4096 vertical quantization levels and 4000 digitized points. These values seem to provide adequate resolution for many applications.

Finally, a ubiquitous source of confusion is simply the difference between the horizontal and vertical magnification of surface profile records. The ratio of vertical to horizontal magnification can be 100:1 or higher in some applications.

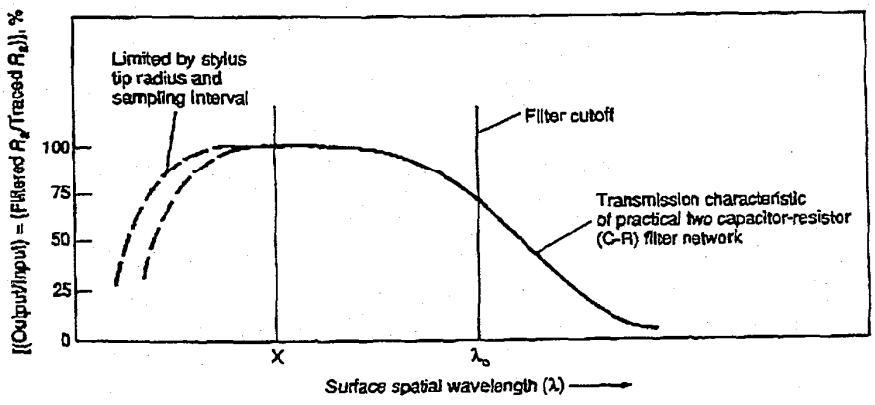

Fig 13 Transmission characteristics of a stylus instrument as a function of surface spatial wavelength. Source: Ref 41

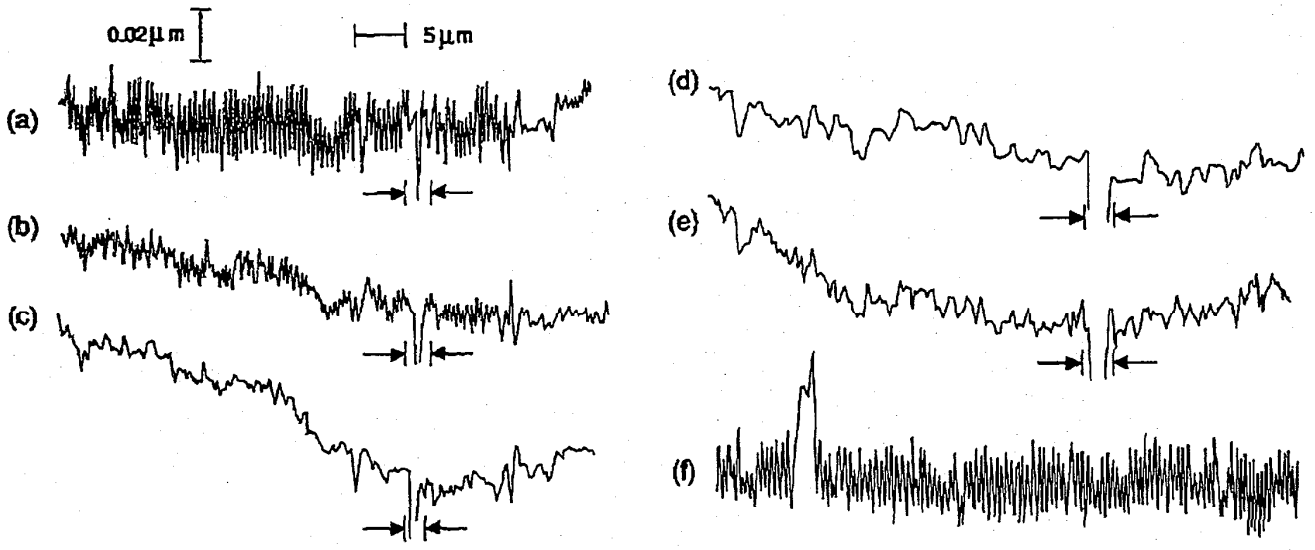

Fig 14 Effect of stylus loading on the surface of a gold grating with 2160 lines/mm. Nominal stylus radius of 0.5 μm (20 μin.). Stylus loading: (a) 0.6 μN. (b) 25 μN. (c) 50 μN. (d) 100 μm. (e) 0.6 μN. (f) 0.6 μN, different position

This effect is not a source of error, but leads to misperceptions of the true appearance of surface texture because the resulting profile records have highly sloped and sharply peaked structures. Figure 15, taken from Reason (Ref 33), shows a comparison between a profile measured with a 1:1 ratio and one with a 25:1 ratio. The qualitative impressions derived from the two pictures are quite different. In reality, surfaces are much less jagged than they appear from conventional profile records.

Examples of Roughness Measurement Results. Of all the surface profiling concepts discussed in this article thus far, the most widely used output parameter is the roughness average, R_a, and perhaps the most important instrument parameter is the long-wavelength cutoff. A few measurement results for R_a from typical metal finishing processes will now be discussed, with the instrument cutoffs noted as well.

The surfaces of metal components can be finished by any of a number of different processes. Typical ranges for the roughness average achieved by a large number of processes are given in Ref 4. The ranges of measurements made by the authors for a few of these processes are shown in Table 1, along with the long-wavelength cutoffs used. These results represent the highest and lowest values that were obtained on roughness comparison surface replicas for each type of finishing process. Nearly all the replicas are commercially available.

The cutoffs were chosen either to be several times longer than the typical spacing produced by the surface finishing process or to be 0.8 mm (0.03 in.) as a minimum. In general, the spacing of the machining marks increases with roughness; therefore, for the same finishing process, rougher surfaces require longer instrument cutoffs.

Ceramic materials are being increasingly used in industrial machinery. Although surface fin-

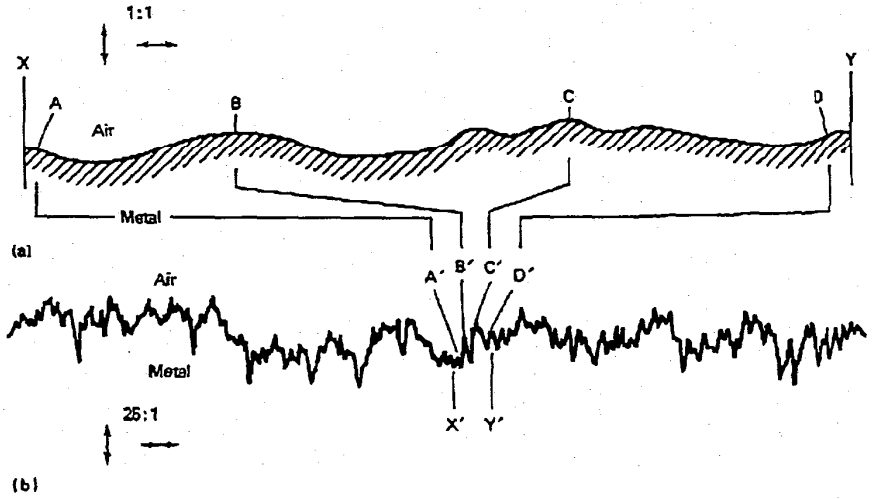

Fig 15 Stylus profiles obtained with two different aspect ratios. (a) Undistorted 1:1 representation. (b) Plot in which the horizontal scale has been compressed by a factor of 25 with respect to the vertical scale Source: Ref 33

Table 1 Extremes of arithmetic average surface roughness, R_a, as a function of selected metalworking finishing processes

	Measured values of surface roughness(a)							
	Minimum				Maximum			
	R_a		Cutoff		R_a		Cutoff	
Finishing process	μm	μin.	mm	in.	μm	μin.	mm	in.
Ground	0.024	0.96	0.8	0.03	3.0	120	0.8	0.03
End milled	1.4	56	0.8	0.03	11	440	No cutoff	
Side milled	1.2	48	2.5	0.10	14	560	No cutoff	
Shaped or turned	0.6	24	0.8	0.03	18	720	2.5	0.1
Electrical discharge machined (EDM)	0.4	16	0.8	0.03	7.5	300	0.8	0.03
Cast	0.9	36	0.8	0.03	72	2900	16	64

(a) For various finishing processes as measured and recorded by J.F. Song and T.V. Vorburger between 1976 and 1991. These values do not necessarily represent the entire range of values obtainable by these processes.

ishing processes are more expensive for ceramics than for metals, the ranges of roughness values achievable for both materials are generally similar. However, many types of ceramic surfaces are porous, and thus the finished surface is characterized by fairly smooth plateaus and deep holes. Therefore, values of skewness tend to be negative, and the values of peak-to-valley parameters tend to be larger relative to R_a for ceramic surfaces than for metal surfaces.

Instrument Calibration

Tribologists often make comparisons of surface texture to determine the existence, extent, and causes of surface wear. These comparisons can be confused by differences in surface measurements taken under different conditions. Are these differences caused by the measuring instruments, the measured surface, or the variation of measuring conditions? How can surface measurements be made accurate and when can they be compared? These questions involve both instrument calibration, correct measuring procedures, and the use of various calibration and check specimens.

General Calibration Issues. The measurement conditions that should be defined, calibrated, or checked for a stylus instrument are (Ref 31, 41, 46):

- Magnification, both in the vertical and horizontal directions
- Stylus tip
- Stylus loading
- Type of skid or reference datum
- Type of filter, reference line, and cutoff length
- Profile digitization
- Algorithms for calculating parameters
- Number and distribution of profiles on the surface

Four types of calibration specimens can be used for this purpose according to ISO standard 5436 (Ref 41): step-height specimens for calibrating the vertical magnification, specimens with fine grooves for checking stylus condition, specimens with periodic profiles for checking vertical and horizontal magnification as well as the character of an electronic filter, and specimens with random profiles for checking the overall response of an instrument (Ref 31, 41).

The vertical magnification of a typical commercial stylus instrument is generally accurate to 10% or better, depending on the fineness of the application. For accurate dimensional measurement of surface structures, the instrument must be calibrated. This is often done by measuring the recorded displacement produced by traversing a step whose height has been calibrated by interferometric measurement. Calibration in the vertical direction becomes difficult at very high magnifications where the desired resolution may be at the nanometer or subnanometer level, somewhat beyond the resolution capabilities of conventional interferometric techniques. In that case, interferometric techniques that incorporate electronic phase measurement (Ref 47) constitute one approach to providing calibrated measurements of small step heights. The sources of uncertainty in surface height calibration and estimates of their magnitudes are discussed elsewhere (Ref 31, 46, 48).

In the lateral direction, the relative displacement of the stylus over the surface can be measured directly by a laser interferometer (Ref 37). Alternatively, calibrated grids or other types of periodic surface specimens (Ref 26) can be used as secondary displacement standards.

Comparison of Roughness Parameters. In order to make surface measurement results comparable, the measurement conditions mentioned above should be precisely defined and specified, especially the stylus size and cutoff length, which limit the bandwidth of the measured profile. The accuracy of surface measurements of manufactured parts is aided further by a well-established measurement procedure, such as the following (Ref 31):

1. Calibrate the vertical magnification of the instrument using a step specimen whose calibrated step height covers the range of surface heights of the engineering surfaces to be measured
2. Verify that the calibration was correct by measuring either the calibrated step height again or a roughness specimen with calibrated R_a, such as a sinusoidal specimen (Ref 27)
3. Measure the engineering surfaces of interest
4. Check the measurement by measuring a check specimen with a waveform identical or similar to that of the measured surface. The R_a or other roughness parameter value of the check specimen should have been calibrated under the same measuring conditions with the same instrument characteristics as the measurement in step 3

In addition, the instrumental parameters, such as filter setting, stylus loading, and straightness of the mechanical motion, should be checked periodically.

Existing roughness calibration specimens can be used as check specimens for a wide range of engineering surface measurements. For example, when the measured engineering surfaces have highly periodic profiles, such as those obtained by turning, planing, or side-milling processes, periodic roughness specimens with triangular, cusped-peak, or sinusoidal profiles can be used as check standards. When the measured engineering surfaces have random profiles, as obtained by grinding, lapping, polishing, and honing processes, the random roughness specimens originating from the Physikalisch Technische Bundesanstalt in Germany (Ref 49) or the Chang Cheng Institute of Metrology and Measurement in China (Ref 40, 50) can be used. These sets combined would cover the range of R_a values from 1.5 to 0.012 μm (59 to 0.5 μin.). If the checking measurement shows that the difference between the measured result for the check specimen and its certified value under reference conditions was within a given tolerance, the measurement of the engineering surface is considered to be under good quality control (Ref 31).

In tribology experiments, if surfaces measured under identical conditions are being compared, the instrument is needed only as a comparator and its absolute calibration is of secondary importance. In such case, only a pilot specimen may be needed for surface measurement quality control. The pilot specimen could be selected from the measured engineering parts or could be an engineering surface with the same surface texture pattern and a similar roughness parameter value as the test surfaces, produced by the same manufacturing process. It should also have good surface texture uniformity. The stylus instrument should be checked for measurement repeatability by measuring the same trace approximately 15 to 20 times. After that, several measurements should be made daily at positions evenly distributed in a small measuring area designated on the surface of the pilot specimen. The user should then be able to detect a significant change in the characteristics of the instrument.

Comparison of the surface profiles often yields more useful information in tribology experiments than the simple comparison of roughness parameters. However, profile comparison requires that the tested surface be relocated in the exact same place from one measurement run to the next. Discrete, recognizable surface features, either natural or artificial, could be used for relocation. In Fig 14, for example, a deep valley on the measured gold grating surface (see arrows) provided a means of orienting these profile graphs from run to run.

Applications

Metalworking. Measurements of surface roughness for metalworking components likely form the bulk of surface roughness measurements throughout the world. The automotive industry is one example where the manufactured surfaces are carefully specified. Table 2, now about 16 years old (Ref 13), shows roughness specifications in terms of the roughness average, R_a, for a number of automobile components. It is likely that these specifications were drawn up empirically and were probably similar to specifications elsewhere in the automotive industry. However, there is no real collective body of knowledge that describes these types of specifications and the reasons for them. As far as can be told, the information is scattered throughout the literature or is proprietary.

Griffiths (Ref 51) attempted to systematize some of the knowledge on surface function. Table 3, taken from his paper, lists the correlations between surface physical properties and various causes of component failure. The circles are taken from previous work of Tonshoff and Brinksmeier (Ref 52) and the squares from Griffiths' additional research. The surface texture influences failure occurring by plastic deformation, fatigue, and corrosion. Griffiths also listed the influence of surface parameters on component performance (Table 4). This table discusses

Table 2 Typical surface roughness specifications of 1976 model year automotive engine components

Component	Manufacturing process	Car No. 1		Car No. 2	
		μm	μin.	μm	μin.
Cylinder block					
Cylinder bore	Honing	0.41-0.51	16-20	0.51-0.64	20-25
Tappet bore	Reaming	1.5-1.9	60-75	2.0-3.0	80-120
Main bearing bore	Boring	1.5-2.0	60-80	3.3-3.8	130-150
Head surface	Milling	1.0-1.3	40-50	4.8-5.3	190-210
Piston					
Skirt	Grinding-polishing	1.1-1.4	45-55	1.0-1.3(a)	40-50(a)
Pin bore	Grinding/polishing	0.76-0.97	30-38	0.28-0.33(a)	11-13(a)
Piston pin	Grinding-lapping	0.23-0.30	9-12	0.08-0.13	3-5
Crankshaft					
Main bearing journal	Grinding-polishing	0.10-0.15	4-6	0.15-0.23	6-9
Connecting rod journal	Grinding-polishing	0.10-0.15	4-6	0.15-0.23	6-9
Camshaft					
Journal	Grinding-polishing	0.10-0.15	4-6	0.36-0.46	14-18
Cam	Grinding-polishing	0.38-0.51	15-20	0.56-0.66(a)	22-26(a)
Rocker arm					
Shaft	Grinding	0.36-0.51	14-20	0.51-0.56	20-22
Bore	Honing-polishing	0.74-0.81	29-32	0.76-1.0	30-40
Valves					
Stem:					
Intake	Grinding	0.86-0.97	34-38	0.41-0.56	16-22
Exhaust	Grinding	0.46-0.51	18-20	0.36-0.51	14-20
Seat:					
Intake	Grinding	0.64-1.0	25-40	0.76-1.0	30-40
Exhaust	Grinding	0.86-1.1	34-45	0.76-0.89	30-35
Tappet					
Face	Grinding	0.10-0.13	4-5	...	
Outside diameter	Grinding	0.36-0.46	14-18	...	
Hydraulic lifter					
Face	Grinding-polishing	0.56-0.64	22-25	0.38-0.51(a)	15-20(a)
Outside diameter	Grinding-polishing	0.36-0.41	14-16	0.23-0.36(a)	13-14(a)

(a) Grinding only; no polishing. Source: Ref 13

Table 3 Effect of surface properties on component failure causes

Cause of failure	Surface physical properties(a)						
	Yield stress	Hardness	Strength	Fatigue strength	Residual stress	Texture	Microcracks
Plastic deformation	●	●				□	
Scuffing/adhesion		●					
Fracture/crack			●				○
Fatigue				●	○	○	●
Cavitation		○					○
Wear		●		□	○		□
Diffusion						○	
Corrosion		□			○	□	●

(a) From original 1980 survey: ●, strong influence; ○, traceable influence; o, supposed influence. Later survey: □, Traceable influence. Source: Ref 51

Table 4 Effect of surface parameters on component performance

Performance parameter	Surface parameter(a)							
	Roughness	Waviness	Form	Lay	Laps and tears	Chemistry	Metallurgy	Stress and hardness
Sealing	●	○		○	○			●
Accuracy	●	○	○		○			●
Cleanliness	●				□	●		
Reflectivity	●	○		○	○	□		
Tool life	●			○	●		●	●
Load carrying	○	●						○
Creep	○					●	○	●
Magnetism						●	●	●
Electrical resistance	●					○	○	
Assembly	○				○	●		○
Fluid flow	●	○		□				
Joints	●	○		○				●

(a) ●, strong influence; o, supposed influence. Source: Ref 51

not only roughness and waviness, but also the metallurgy and chemistry of the surfaces and other qualities as well. Roughness is particularly important for sealing, dimensional accuracy preserving the cleanliness of the component, optical reflectivity, and several other functions.

Tribology and Wear. An important research direction in tribology is to determine the relationship between surface texture and wear properties, and the variation of surface texture during the wear process. Many investigators use standard test geometries for wear and friction tests, such as pin-on-disk or four-ball tests (Ref 53-56). The amount and structure of damage to these components is of great interest in such tests. Key measurable parameters are the volume of material removed by wear and the surface area of the wear scar.

As discussed by Whitenton and Blau (Ref 55), both two-dimensional analysis of profiles and three-dimensional analysis of surface topography maps can be used to assess wear damage. In the two-dimensional approach, a profile of the wear scar is obtained and the area lost or gained in the wear region is estimated. By projection, the volume can be estimated as well. The profile can be obtained by stylus measurements or by image analysis of the scar.

In the three-dimensional approach, the measurement system generates a matrix of X, Y, and Z values that describe the topography of the surface after the test. Parameters such as surface area can be determined from this matrix. In addition, the volume removed by wear can be obtained by comparing the surface map with that for the unworn surface. An important advantage of this method is its accuracy; it produces the most direct measurement of the wear volume. One disadvantage is that it is more time consuming than the two-dimensional method.

Figure 16 shows the surface topography that resulted from measuring a bottom ball in a four-ball test (Ref 56) that used 6.35 mm (0.25 in.) radius α-alumina balls. These three-dimensional data of the wear scar surface were carefully filtered to remove extraneous instrumental errors.

Figure 17 shows the relationship between the wear volume of the top ball scars and the bottom ball scars in the four-ball test. Five sets of balls were tested at room temperature while immersed in paraffin oil. Because there are three bottom balls which wear simultaneously, three times the wear volume for one ball is plotted along the x-axis. The scar volume of the top ball is plotted along the y-axis. Under the five different sets of experimental conditions, the total wear volume lost for the bottom ball scars as calculated from surface profiling appears to be about equal to the wear volume lost for the top ball scar.

Another application of surface texture measurements in tribology is the examination of used components to gain information on the wear mechanism (Ref 57). For example, the mechanism of scuffing involves the destruction of surfaces by the welding and fracture of asperity contacts. Such surfaces are easily distinguished from those produced by controlled running-in wear. Many engines use specially formulated

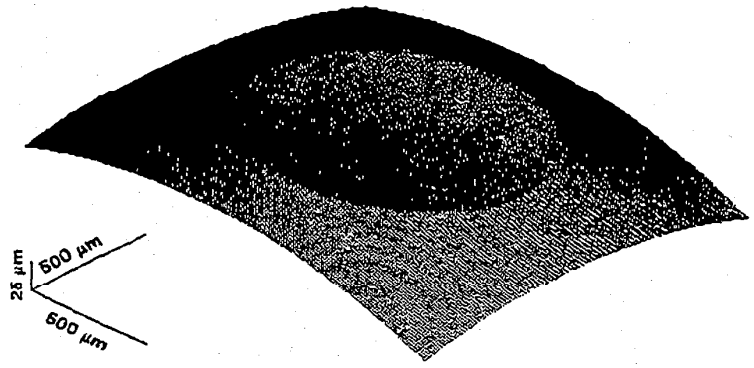

Fig 16 Bottom-ball topographic data for a four-ball test showing a round wear scar. Source: Ref 56

"first-fill" lubricants designed to assist the running-in of the surfaces. This running-in is crucial for obtaining satisfactory service life.

Bovington (Ref 57) has observed how a properly run-in surface can be distinguished from a scuffed surface. Generally, the run-in surface contains a number of flat plateaus, the peak-valley roughness is about half that of the new surface, and the skewness, R_{sk}, is negative. Running-in proceeds in a controlled manner, that is, with the truncation of surface peaks but without abrasive or adhesive wear processes. The truncations or plateaus result in a reduction of the contact pressures, and their presence is a good indication of long service life. Scuffing, on the other hand, generates new surfaces. Therefore, the peak-valley roughness does not decrease, and the R_{sk} parameter does not become progressively more negative.

Bovington (Ref 57) has also observed that modern engine design and lubrication technology are so advanced that the old methods of evaluation of wear, such as weight loss, are becoming irrelevant. The lubricant industry needs to begin defining wear in terms of changes in surface texture.

Davis *et al.* (Ref 58) measured the three-dimensional topography of various places in a honed engine cylinder bore and related the topography to component wear. Based on detailed results, they developed a chart showing oil volume in cubic millimeters versus the amount of the surface that would be truncated by the wearing process. The oil volume is related to the volume of the surface valleys, calculated from their three-dimensional topographic measurements. Their mathematical truncation process was a simulation of a wear process that cuts off the surface peaks. For an engine cylinder bore, oil volume is of crucial importance. Figure 18 shows data taken from the analyses of one of their three-dimensional topographic maps. As the truncation proceeds, the oil volume in the valleys decreases. Based on their information and measurement results, Davis *et al.* (Ref 58) predicted that the component would begin to fail at a truncation level between 60 to 70%, because the oil volume would decrease to unacceptable levels.

Magnetic Storage. Tribology is especially important to the functioning of tapes and disks in the magnetic recording industry (Ref 59), including the hydrodynamic properties of flying read heads, the lubrication of tapes and disks, and the sliding contact between a disk and a read head upon startup. Surface roughness is also important. Figure 19 shows results from Bhushan *et al.* (Ref 59, 60) for the measured coefficient of friction of six CrO_2 magnetic tapes sliding against a glass head as a function of the rm roughness measured with an optical profile The tapes all had the same composition; the vari ation in rms roughness was achieved by usin different calendering pressures during the finish ing process. The coefficient of friction de creased rapidly up to an rms roughness of abo 40 nm, then seemed to remain fairly level. How ever, when the friction results were plotted ve sus the real area of contact (normalized to th applied load), an excellent linear correlation wa obtained (Fig 19b). The quantity plotted alon the abscissa is based on Greenwood an Williamson's formula (Ref 15) for the real are of contact, A_r, in the elastic regime:

$$\frac{A_r}{A_a p_a} = \frac{3.2}{E^* \left(\frac{\sigma_p}{R_p}\right)^{1/2}} \qquad \text{(Eq 1}$$

where A_a is the apparent area of contact, p_a is t apparent pressure, σ_p is the standard deviati of the composite peak-height distribution of t contacting surfaces, R_p is the composite pe curvature of the contacting surfaces, and E^* i composite modulus that is a function of t Young's modulus and Poisson's ratio of the co tacting materials. The linear relationship o tained by Bhushan *et al.* (Ref 59, 60) was du cated by Miyoshi *et al.* (Ref 61) for the same magnetic tapes sliding on a nickel-zinc fer pin in a pin-on-flat experiment.

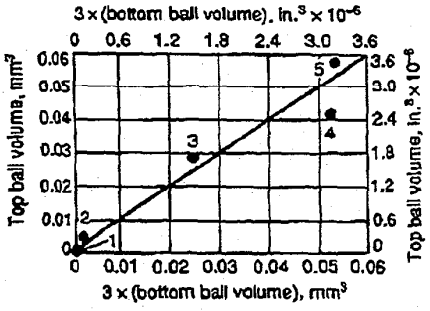

Fig 17 Relation of the wear volumes of the top-ball wear scars to the bottom-ball wear scars. Because there are three bottom balls, three times the wear volume for one ball is plotted along the x-axis. The top-ball scar volume is plotted along the y-axis. A 1:1 45° line is also drawn. The numbered data points correspond to the test numbers. Source: Ref 56

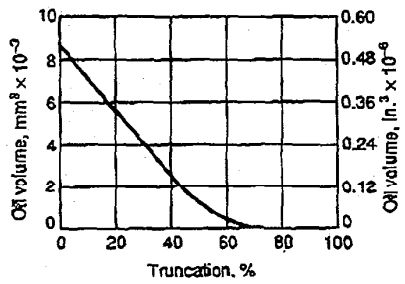

Fig 18 Oil volume for cylinder bores estimated by mathematical truncation of a surface topography map. Source: Ref 58

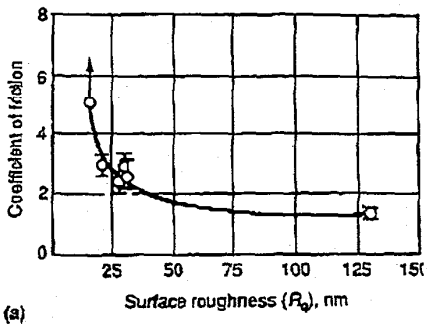

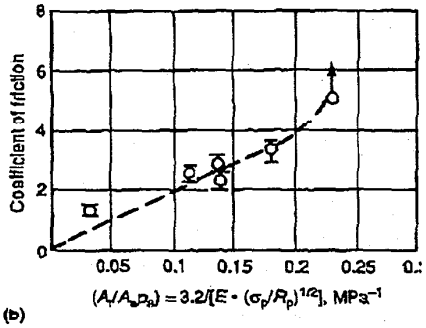

Fig 19 Coefficient of friction for six CrO_2 magneti tapes as a function of two parameters. (a Coefficient of friction versus rms roughness, R_q. (b Coefficient of friction versus the real area of contac A_r (normalized to contact load). Source: Ref 59, 60

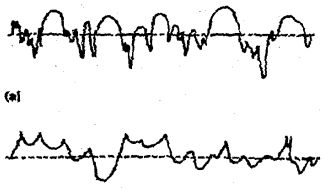

(a)

(b)

Fig 20 Reconstructions from pattern recognition analysis of profiles of the contacting surface of lip seals. (a) Ideally good seal. (b) Ideally bad seal. Source: Ref 63

Lip Seals. Thomas *et al.* (Ref 62, 63) used pattern recognition techniques to correlate surface texture and lip sealing performance. They measured surface profiles of a set of rubber lip seals, some good and some leaky, and calculated a number of surface parameters from the profiles, such as R_a, R_{sk}, and peak curvature. The groups of parameters for the good and bad seals were then separated by pattern recognition techniques. From these results, they constructed model profiles for successful and leaky sealing surfaces (Fig 20). Although this approach is highly empirical, it can lead to a sound understanding of surface function by enabling the engineer to focus on the most probable parameters affecting performance.

Wherever possible, engineering surfaces should be assessed by evaluating those surface parameters that strongly correlate with the component function. The type and control values of these functional parameters can be determined by controlled experiments. This example of lip seals again highlights the importance of surface texture design (Ref 31). The functional performance of engineering surfaces can be optimized in a comprehensive way by proper design of their surface texture, specification of the material and manufacturing process, and development of quality control procedures.

REFERENCES

1. Elements of this article have been presented in T.V. Vorburger and G.G. Hembree, "Characterization of Surface Topography," Navy Metrology R&D Program Conference Report, U.S. Department of the Navy (Corona, CA), April 1989, and in Ref 2
2. T.V. Vorburger and J. Raja, "Surface Finish Metrology Tutorial," NISTIR 89-4088, National Institute of Standards and Technology, 1990
3. T.R. Thomas, Ed., *Rough Surfaces*, Longman, London, 1982, p 189
4. "Surface Texture (Surface Roughness, Waviness, and Lay)," ANSI/ASME B46.1-1985, American Society of Mechanical Engineers, 1985
5. "Instruments for the Measurement of Surface Roughness by the Profile Method—Vocabulary," ISO 1879/1981, International Organization for Standardization, 1981
6. D.J. Whitehouse, *Characterization of Solid Surfaces*, P.E. Kane and G.R. Larrabee, Ed., Plenum Press, 1975, p 49-73
7. J.M. Bennett and J.H. Dancy, Stylus Profiling Instrument for Measuring Statistical Properties of Smooth Optical Surfaces, *Appl. Opt.*, Vol 20, 1981, p 1785
8. B. Scheffer and C. Thurel, Données de base de la Realisation d'un Calculateur R et W, *Méc. Matér. Electr.*, Vol 286, 1973, p 19
9. J. Bielle, Functional Needs, Machining Conditions, and Economics of Surface Finishing, *Prec. Eng.*, Vol 7, 1985, p 31
10. D.J. Whitehouse, The Parameter Rash—Is There a Cure?, *Wear*, Vol 83, 1982, p 75
11. J.M. Bennett and L. Mattsson, *Introduction to Surface Roughness and Scattering*, Optical Society of America, 1989
12. P.K. Hansma, V.B. Elings, O. Marti, and C.E. Bracker, Scanning Tunneling Microscopy and Atomic Force Microscopy: Application to Biology and Technology, *Science*, Vol 242, 1988, p 209
13. R.D. Young, "The National Measurement System for Surface Finish," NBSIR 75-927, National Bureau of Standards, 1976
14. "Surface Roughness—Terminology—Part 1: Surface and Its Parameters," ISO 4287/1, International Organization for Standardization, 1984
15. J.A. Greenwood and J.B.P. Williamson, Contact of Nominally Flat Surfaces, *Proc. R. Soc. (London) A*, Vol A295, 1966, p 300
16. A.W. Bush and R.D. Gibson, A Theoretical Investigation of Thermal Contact Conductance, *Appl. Energy*, Vol 5, 1979, p 11
17. P.R. Nayak, Random Process Model of Rough Surfaces, *J. Lubr. Technol. (Trans. ASME)*, Vol 93, 1971, p 398
18. J.S. Bendat and A.G. Piersol, *Random Data: Analysis and Measurement Procedures*, Wiley-Interscience, 1971
19. M.S. Longuet-Higgins, The Statistical Analysis of a Random, Moving Surface, *Trans. R. Soc. (London) A*, Vol 249A, 1957, p 321
20. R.B. Blackman and J.W. Tukey, *The Measurement of Power Spectra*, Dover, 1959
21. R.S. Sayles, *Rough Surfaces*, T.R. Thomas, Ed., Longman, London, 1982, chap 3
22. J.B.P. Williamson, *Rough Surfaces*, T.R. Thomas, Ed., Longman, London, 1982, chap 1
23. J.M. Elson and J.M. Bennett, Relation Between the Angular Dependence of Scattering and the Statistical Properties of Optical Surfaces, *J. Opt. Soc. Am.*, Vol 69, 1979, p 31
24. E.O. Brigham, *The Fast Fourier Transform*, Prentice-Hall, 1974, chap 10
25. T.V. Vorburger, "FASTMENU: A Set of FORTRAN Programs for Analyzing Surface Texture," NBSIR 83-2703, National Bureau of Standards, 1983, chap 11
26. R.L. McKenzie, Ed., "NIST Standard Reference Materials Catalog 1990–1991," National Institute of Standards and Technology, 1990, p 124
27. E.C. Teague, F.E. Scire, and T.V. Vorburger, Sinusoidal Profile Precision Roughness Specimens, *Wear*, Vol 83, 1982, p 61
28. E.L. Church, T.V. Vorburger, and J.C. Wyant, Direct Comparison of Mechanical and Optical Measurements of the Finish of Precision Machined Optical Surfaces, *Opt. Eng.*, Vol 24, 1985, p 388
29. K.J. Stout and E.J. Davis, Surface Topography of Cylinder Bores—Relationship Between Manufacture, Characterization, and Function, *Wear*, Vol 95, 1984, p 111
30. "Measurement of Surface Roughness, Parameter R_k, R_{pk}, R_{vk}, M_{r1}, M_{r2} for the Description of the Material Portion (Profile Bearing Length Ratio) in the Roughness Profile," DIN 4776-1985, Deutsches Institut für Normung, 1985
31. J.F. Song and T.V. Vorburger, Standard Reference Specimens in Quality Control of Engineering Surfaces, *J. Res. Natl. Inst. Stand. Technol.*, Vol 96, 1991, p 271
32. D.W. Blakely and G.A. Somorjai, The Dehydrogenation and Hydrogenolysis of Cyclohexane and Cyclohexene on Stepped (High Miller Index) Platinum Surfaces, *J. Catal.*, Vol 42, 1976, p 181
33. R.E. Reason, *Modern Workshop Technology*, Vol 2, *Processes*, 3rd ed., H.W. Baker, Ed., Macmillan, 1970, chap 23
34. J.D. Garratt, New Stylus Instrument With a Wide Dynamic Range for Use in Surface Metrology, *Prec. Eng.*, Vol 4, 1982, p 143
35. R.E. Reason, Surface Finish and Its Measurement, *J. Inst. Prod. Eng.*, Vol 23, 1944, p 347
36. J.B. Bryan, The Abbé Principle Revisited—An Updated Interpretation, *Prec. Eng.*, Vol 1, 1979, p 129
37. E.C. Teague, R.D. Young, F.E. Scire, and D. Gilsinn, Para-Flex Stage for Microtopographic Mapping, *Rev. Sci. Instrum.*, Vol 59, 1988, p 67
38. T.V. Vorburger, E.C. Teague, F.E. Scire, and F.W. Rosberry, Measurements of Stylus Radii, *Wear*, Vol 57, 1979, p 39
39. J.F. Song and T.V. Vorburger, Stylus Profiling at High Resolution and Low Force, *Appl. Opt.*, Vol 30, 1991, p 42
40. J.F. Song, Random Profile Precision Roughness Calibration Specimens, *Surf. Topog.*, Vol 1, 1988, p 303
41. Calibration Specimens—Stylus Instruments—Types, Calibration and Use of Specimens, ISO 5436-1985, International Organization for Standardization, 1985
42. T.R. Thomas, Ed., *Rough Surfaces*, Longman, London, 1982, p 24-25
43. M.N.H. Darnir, Error in Measurement Due to Stylus Kinematics, *Wear*, Vol 26, 1973, p 219
44. S. Ajioka, The Dynamic Response of Stylus, *Bull. Jpn. Soc. Prec. Eng.*, Vol 1, 1966, p 228
45. J.I. McCool, Assessing the Effect of Stylus

Tip Radius and Flight on Surface Topography Measurements, *J. Tribology (Trans. ASME)*, Vol 202, 1984

46. E.C. Teague, "Evaluation, Revision, and Application of the NBS Stylus/Computer System for the Measurement of Surface Roughness," Tech. Note 902, National Bureau of Standards, 1976
47. J.C. Wyant, C.L. Koliopoulos, B. Bhushan, and O.E. George, An Optical Profilometer for Surface Characterization of Magnetic Media, *ASLE Trans.*, Vol 27, 1984, p 101; and B. Bhushan, J.C. Wyant, and C.L. Koliopoulos, Measurement of Surface Topography of Magnetic Tapes by Mirau Interferometry, *Appl. Opt.*, Vol 24, 1985, p 1489
48. T.V. Vorburger, "Appendix A: Measurement Conditions and Sources of Uncertainty for NIST Roughness and Step Height Calibration Reports," unpublished
49. J. Hasing, Herstellung und Eigenschaften von Referenznormalen für das Einstellen von Oberflachenmessgeraten, *Werkstattstechnik*, Vol 55, 1965, p 380
50. J.F. Song, T.V. Vorburger, and P. Rubert, Comparison Between Precision Roughness Master Specimens and Their Electroformed Replicas, *Prec. Eng.*, Vol 14, 1992, p 84
51. B.J. Griffiths, Manufacturing Surface Design and Monitoring for Performance, *Surf. Topog.*, Vol 1, 1988, p 61
52. H.K. Tonshoff and E. Brinksmeier, Determination of the Mechanical and Thermal Influences on Machined Surfaces by Microhardness and Residual Stress Analysis, *CIRP Ann.*, Vol 29 (No. 2), 1980, p 519
53. P.A. Willermet and S.K. Kandah, Wear Asymmetry—A Comparison of the Wear Volumes of the Rotating and Stationary Balls in the Four-Ball Machine, *ASLE Trans.*, Vol 26, 1982, p 173
54. I.M. Feng, A New Approach in Interpreting the Four-Ball Wear Results, *Wear*, Vol 5, 1962, p 275
55. E.P. Whitenton and P.J. Blau, A Comparison of Methods for Determining Wear Volumes and Surface Parameters of Spherically Tipped Sliders, *Wear*, Vol 124, 1988, p 291
56. E.P. Whitenton and D.E. Deckman, Measuring Matching Wear Scars on Balls and Flats, *Surf. Topog.*, Vol 2, 1989, p 205
57. C.H. Bovington, Surface Finish and Engine Testing of Lubricants: An Industrialist View, *Surf. Topog.*, Vol 1, 1988, p 483
58. E.J. Davis, P.J. Sullivan, and K.J. Stout The Application of 3-D Topography to Engine Bore Surfaces, *Surf. Topog.*, Vol 1 1988, p 63; K.J. Stout, E.J. Davis, and P.J Sullivan, *Atlas of Machined Surfaces* Chapman and Hall, London, 1990
59. B. Bhushan, *Tribology and Mechanics o Magnetic Storage Devices*, Springer-Ver lag, 1990
60. B. Bhushan, R.L. Bradshaw, and B.S Sharma, Friction in Magnetic Tapes II Role of Physical Properties, *ASLE Trans.* Vol 27, 1984, p 89
61. K. Miyoshi, D.H. Buckley, and B. Bhushan, "Friction and Morphology of Magnetic Tapes in Sliding Contact With Nickel-Zinc Ferrite," Technical Paper 2267, National Aeronautics and Space Administration 1984
62. T.R. Thomas, C.F. Holmes, H.T. McAdams, and J.C. Bernard, "Surface Features Influencing the Effectiveness of Lip Seals A Pattern Recognition Approach," Technical Paper IQ75-128, Society of Manufacturing Engineers, 1975
63. T.R. Thomas and R.S. Sayles, *Rough Surfaces*, T.R. Thomas, Ed., Longman, London, 1982, p 231-233